Probing sensitivity to charged scalars through partial differential widths: $\tau \to K\pi\pi\nu_\tau$ decays

Nicolas Mileo,[1,*] Ken Kiers,[2,†] and Alejandro Szynkman[1,‡]

[1]*IFLP, CONICET – Dpto. de Física, Universidad Nacional de La Plata, C.C. 67, 1900 La Plata, Argentina*
[2]*Physics and Engineering Department, Taylor University,*
236 West Reade Avenue, Upland, Indiana 46989, USA
(Received 20 October 2014; published 9 April 2015)

We define and test CP-even and CP-odd partial differential widths for the process $\tau \to K\pi\pi\nu_\tau$ assuming that an intermediate heavy charged scalar contributes to the decay amplitude. Adopting a model-independent approach, we use a Monte Carlo simulation in order to study the number of events needed to recover information on the new physics from these observables. Our analysis of the CP-odd observables indicates that the magnitude of $f_H\eta_P$, which is related to the new-physics contribution, can be recovered with an uncertainty smaller than 3% for 3×10^6 events. This number of events would also allow one to retrieve certain parameters appearing in the Standard Model amplitude at the percent level. In addition, we discuss the possibility of using the proposed observables to study specific models involving two Higgs doublets, such as the aligned two-Higgs-doublet model. This analysis is undertaken within the context of the upcoming super B-factories, which are expected to provide a considerably larger number of events than that which was supplied by the B-factories. Moreover, a similar set of observables could be employed to study other decay modes such as $\tau \to \pi\pi\pi\nu_\tau$, $\tau \to KK\pi\nu_\tau$ and $\tau \to KKK\nu_\tau$.

I. INTRODUCTION

With the discovery of a new boson H by the ATLAS [1] and CMS [2] collaborations, it is now very important to characterize this new particle in order to study the extent to which its features are in agreement with those predicted for the Higgs scalar within the Standard Model (SM). In particular, the spin of this new boson and its couplings to other particles have been carefully analyzed giving rise, with a high degree of confidence, to the conclusion that it has spin zero and that its couplings to the other particles are linearly correlated with their masses (see Refs. [3,4] and references therein). On the other hand, the possibility of an enlarged scalar spectrum is also being tested. In particular, from the high energy point of view, many searches for charged Higgs bosons decaying via $H \to \tau\nu_\tau$ have been performed by ATLAS and CMS (see, for example, Refs. [5–7]). These searches have found the data to be consistent with the expected SM background and have set limits on the branching ratio of top quark decays to a b quark and a charged Higgs boson. The effects of the presence of a charged Higgs boson can also be studied indirectly by means of low energy observables defined, for example, for leptonic and semileptonic decays involving B, D^*, D, D_s, K, and π mesons [8]. Such decays have been widely studied at the B-factories by the Belle and *BABAR* collaborations. Moreover, the fact that no new particle has been observed at the present time may suggest that the new-physics (NP) scale is out of reach for the LHC. Indirect searches for physics beyond the SM become particularly important within this context.

Among the various processes that can receive contributions from a charged Higgs boson, the τ lepton decays can be used to derive constraints on the scalar and pseudoscalar couplings of a charged scalar to fermions. The fact that CP-violating effects are expected to be negligible within the SM means that a study of CP-odd observables could reveal the presence of contributions from a charged Higgs boson, should the charged Higgs-fermion couplings violate CP. Such an analysis has been carried out for the decay $\tau \to K\pi\pi\nu_\tau$ in Ref. [9], where the presence of a charged scalar contributing to the corresponding amplitude is assumed and two types of CP-asymmetries are defined in addition to the usual partial rate asymmetry. In the present work, which extends the analysis of Ref. [9], we focus on the same decay $\tau \to K\pi\pi\nu_\tau$, with the main goal being to define and test various CP-even and CP-odd observables, on the one hand, and to study their sensitivity to a NP contribution due to the presence of a charged scalar, on the other. The decay under consideration, $\tau \to K\pi\pi\nu_\tau$, only involves a pseudoscalar coupling of a charged scalar to the up and strange quarks, in contrast to $\tau \to K\pi\nu_\tau$, for instance, which exclusively probes the scalar coupling [10]. It is also worth noting that the simplest τ decay with $\Delta S = 1$ that probes the contribution arising from the exchange of a charged scalar is $\tau \to K\nu_\tau$. In fact, this decay involves exactly the same pseudoscalar coupling as $\tau \to K\pi\pi\nu_\tau$ and then imposes constraints on it.

*[*]mileo@fisica.unlp.edu.ar
[†]knkiers@taylor.edu
[‡]szynkman@fisica.unlp.edu.ar

For the analysis of the observables introduced below, we use a large number of Monte Carlo simulated events. The size of the Monte Carlo sample has been chosen within the context of the upcoming super B-factories, which are expected to significantly increase the luminosity as compared to the B-factories. The aim of this analysis is to provide insight into the number of events needed to extract information about the NP contribution as well as about the SM contributions, including the anomalous Wess-Zumino (W-Z) term.

Although our primary focus in the present work is on a model-independent treatment of charged-scalar contributions to $\tau \to K\pi\pi\nu_\tau$, it is useful also to consider a specific scenario. Many models include one additional Higgs doublet, so that a charged Higgs is present. In particular, in the so-called aligned two-Higgs-doublet model (A2HDM), an alignment in flavor space of the Yukawa couplings of the two scalar doublets is enforced, leading to the elimination of flavor-changing neutral currents at tree level. This restrictive choice results in a highly predictive phenomenology for this model, which has been carefully explored (see Refs. [11–13]). Of particular interest to us is not only the fact that the A2HDM includes potential new sources of CP violation but also that it imposes very restrictive constraints due to the three-family universality of the proportionality constants arising from the alignment in flavor space. The partial differential widths studied in this work can be considered as additional observables to test the A2HDM, specifically within the context of the super B-factories, in which the possibility of extracting these distributions from the data is more plausible. In this paper we briefly discuss the usefulness of the proposed observables to probe the A2HDM.

The remainder of this paper is organized as follows. In Sec. II we write down the expression for the differential width for the decay $\tau^- \to K^-\pi^-\pi^+\nu_\tau$ in terms of the corresponding form factors, including both the NP and SM contributions. By integrating the differential width weighted by various angular functions, we define partial differential widths in Sec. III. Section IV introduces a set of CP-even and CP-odd observables derived from the weighted partial widths. The parametrization for the form factors, along with the set of reference values used later for the event simulation, are summarized in Sec. V. The analysis of the proposed CP-even and CP-odd observables is included in Sec. VI. Finally, in Sec. VII the decay is considered in the context of the A2HDM, and in Sec. VIII some possibilities of testing the different assumptions used during the paper are briefly discussed. We summarize the main conclusions in Sec. IX. The Appendix contains some details relevant for the statistical analysis.

II. DIFFERENTIAL WIDTH FOR $\tau^- \to K^-\pi^-\pi^+\nu_\tau$

We start with the effective Hamiltonian that accounts for the decay $\tau^- \to K^-\pi^-\pi^+\nu_\tau$ within the SM,

$$\mathcal{H}_{\text{eff}}^{\text{SM}} = \frac{G_F}{\sqrt{2}}\sin\theta_c[\bar{\nu}_\tau\gamma_\mu(1-\gamma_5)\tau][\bar{s}\gamma^\mu(1-\gamma_5)u] + \text{H.c.}, \quad (1)$$

where G_F is the Fermi constant and θ_c is the Cabibbo angle. Possible NP effects due to a new charged scalar boson contributing to the decay may be included by adding the following terms to the effective Hamiltonian,

$$\mathcal{H}_{\text{eff}}^{\text{NP}} = \frac{G_F}{\sqrt{2}}\sin\theta_c[\eta_S\bar{\nu}_\tau(1+\gamma_5)\tau\bar{s}u + \eta_P\bar{\nu}_\tau(1+\gamma_5)\tau\bar{s}\gamma_5u]$$
$$+ \text{H.c.}, \quad (2)$$

where η_S and η_P are the scalar and pseudoscalar couplings, respectively. The hadronic matrix element $J^\mu \equiv \langle K^-(p_1)\pi^-(p_2)\pi^+(p_3)|\bar{s}\gamma^\mu(1-\gamma_5)u|0\rangle$ can be conveniently parametrized in terms of four form factors as

$$J^\mu = [F_1(Q^2,s_1,s_2)(p_1-p_3)_\nu + F_2(Q^2,s_1,s_2)(p_2-p_3)_\nu]T^{\mu\nu}$$
$$+ iF_3(Q^2,s_1,s_2)\epsilon^{\mu\nu\rho\sigma}p_{1\nu}p_{2\rho}p_{3\sigma} + F_4(Q^2,s_1,s_2)Q^\mu,$$
$$(3)$$

where $Q^\mu = (p_1 + p_2 + p_3)^\mu$, $T^{\mu\nu} = g^{\mu\nu} - Q^\mu Q^\nu/Q^2$, $s_1 = (p_2 + p_3)^2$, and $s_2 = (p_1 + p_3)^2$ and where we adopt the convention $\epsilon_{0123} = +1$, as in Refs. [9,14]. The functions $F_1 - F_4$ are the form factors that arise from the different possible decay chains. F_1 and F_2 appear due to the decay chains involving the $K_1(1270)$ and $K_1(1400)$ resonances, F_3 is the anomalous Wess-Zumino term, and F_4 is the scalar form factor, which is generally assumed to be negligible for this decay since there is no pseudoscalar resonance through which the decay can proceed [15]. The axial vector form factors F_1 and F_2 give the dominant contributions, while the anomalous vector form factor F_3 represents a subdominant contribution, as shown by numerical estimates [10]. The NP contribution coming from a scalar boson can be incorporated into the amplitude through the shift $F_4 \to \tilde{F}_4 = F_4 + f_H\eta_P/m_\tau$ [9], where the pseudoscalar form factor f_H is defined as

$$f_H = \langle K^-(p_1)\pi^-(p_2)\pi^+(p_3)|\bar{s}\gamma_5u|0\rangle. \quad (4)$$

The starting point for our analysis will be the differential width for the decay obtained from Eq. (25) in Ref. [9] after integrating over the angle θ. The angle θ is defined in the rest frame of the tau; it is the angle between the direction of the hadrons ("$\vec{Q}$") in that frame and the direction of the tau in the laboratory frame. Performing the integration, we obtain

$$\frac{d\Gamma}{dQ^2 ds_1 ds_2 d\gamma d\cos\beta} = \frac{A(Q^2)}{4\pi}\left\{\left[\frac{2}{3}\langle K_1\rangle + \langle K_2\rangle + \frac{1}{3}\langle\overline{K}_1\rangle(3\cos^2\beta - 1)/2\right](|B_1|^2 + |B_2|^2)\right.$$

$$+ \left[\frac{2}{3}\langle K_1\rangle + \langle K_2\rangle - \frac{2}{3}\langle\overline{K}_1\rangle(3\cos^2\beta - 1)/2\right]|B_3|^2 + \langle K_2\rangle|B_4|^2$$

$$- \frac{1}{2}\langle\overline{K}_1\rangle\sin^2\beta\cos 2\gamma(|B_1|^2 - |B_2|^2) + \langle\overline{K}_1\rangle\sin^2\beta\sin 2\gamma\mathrm{Re}(B_1 B_2^*)$$

$$+ 2\langle\overline{K}_3\rangle\sin\beta\sin\gamma\mathrm{Re}(B_1 B_3^*) + 2\langle\overline{K}_2\rangle\sin\beta\cos\gamma\mathrm{Re}(B_1 B_4^*)$$

$$+ 2\langle\overline{K}_3\rangle\sin\beta\cos\gamma\mathrm{Re}(B_2 B_3^*) - 2\langle\overline{K}_2\rangle\sin\beta\sin\gamma\mathrm{Re}(B_2 B_4^*)$$

$$+ 2\langle\overline{K}_3\rangle\cos\beta\mathrm{Im}(B_1 B_2^*) + \langle\overline{K}_1\rangle\sin 2\beta\cos\gamma\mathrm{Im}(B_1 B_3^*)$$

$$\left. - \langle\overline{K}_1\rangle\sin 2\beta\sin\gamma\mathrm{Im}(B_2 B_3^*) + 2\langle\overline{K}_2\rangle\cos\beta\mathrm{Im}(B_3 B_4^*)\right\}, \tag{5}$$

where

$$A(Q^2) = \frac{G_F^2 \sin^2\theta_c}{128(2\pi)^5}\frac{(m_\tau^2 - Q^2)^2}{m_\tau^3 Q^2}, \tag{6}$$

and

$$\langle K_i\rangle \equiv \frac{1}{2}\int_0^\pi K_i \sin\theta d\theta \tag{7}$$

(and similarly for $\langle\overline{K}_i\rangle$); the definitions of the K_i and the $\overline{K}_i$ may be found in Ref. [9]. As described in Ref. [9] (the definitions therein are identical to those in Ref. [14]), β and γ are Euler angles relating two coordinate systems used to specify the kinematics of the decay. Moreover, the functions $B_1 - B_4$ are linearly related to the form factors as follows:

$$B_1 = [F_1(p_1 - p_3)^x + F_2(p_2 - p_3)^x] \tag{8}$$

$$B_2 = (F_1 - F_2)p_1^y \tag{9}$$

$$B_3 = F_3\sqrt{Q^2}\,p_1^y p_3^x \tag{10}$$

$$B_4 = \sqrt{Q^2}\left[F_4 + \frac{f_H}{m_\tau}\eta_P\right]. \tag{11}$$

Note that the form factors F_i and f_H are potential sources of strong phases and that the only possible weak phase comes from the pseudoscalar coupling η_P. For future reference, let us also define the quantity $\overline{B}_4$, which is relevant for τ^+ decays,

$$\overline{B}_4 = \sqrt{Q^2}\left[F_4 + \frac{f_H}{m_\tau}\eta_P^*\right]. \tag{12}$$

In fact, the differential width for the *CP*-conjugate decay $\tau^+ \to K^+\pi^+\pi^-\bar{\nu}_\tau$ can be obtained by replacing B_4 by $\overline{B}_4$ in Eq. (5) since the only source of *CP* violation appears in B_4

through the coupling η_P. For further details of the quantities involved within this section, see Ref. [9].

III. WEIGHTED DIFFERENTIAL WIDTHS

We now define observables that exploit the angular information that is available in the expression for the differential width. To do so, we employ weighting functions that allow us to isolate different contributions. Inspection of Eq. (5) reveals that it depends on nine different functions of the angles β and γ. These functions form an orthogonal set; the functions, and their normalizations, are shown in Table I. The orthogonality of the functions means that different terms in Eq. (5) can be easily isolated by performing angular integrations of the differential width weighted by these angular functions. Hence, we can define nine weighted differential widths,

$$\frac{d\Gamma_i}{dQ^2 ds_1 ds_2} \equiv \int \frac{d\Gamma}{dQ^2 ds_1 ds_2 d\gamma d\cos\beta}h_i(\gamma,\beta)\sin\beta d\beta d\gamma,$$

$$i = 1,\ldots,9. \tag{13}$$

It is straightforward to perform the integrations in Eq. (13) using the information from Table I. The results for the

TABLE I. Angular weighting factors. The $h_i(\gamma,\beta)$ functions form an othogonal set. The normalization factors are given in the third column.

i	$h_i(\gamma,\beta)$	$\iint[h_i(\gamma,\beta)]^2 \sin\beta d\gamma d\beta$
1	1	4π
2	$3\cos^2\beta - 1$	$16\pi/5$
3	$\sin^2\beta\cos 2\gamma$	$16\pi/15$
4	$\sin^2\beta\sin 2\gamma$	$16\pi/15$
5	$\sin\beta\sin\gamma$	$4\pi/3$
6	$\sin\beta\cos\gamma$	$4\pi/3$
7	$\cos\beta$	$4\pi/3$
8	$\sin 2\beta\cos\gamma$	$16\pi/15$
9	$\sin 2\beta\sin\gamma$	$16\pi/15$

TABLE II. Weighted partial widths for the τ^- decay. The related expressions for the CP-conjugate decay may be obtained by replacing B_4 by $\overline{B}_4$ everywhere it appears.

i	$(d\Gamma_i/dQ^2ds_1ds_2)/A(Q^2)$
1	$(\frac{2}{3}\langle K_1\rangle + \langle K_2\rangle)(|B_1|^2 + |B_2|^2 + |B_3|^2) + \langle K_2\rangle|B_4|^2$
2	$\frac{2}{15}\langle \overline{K}_1\rangle(|B_1|^2 + |B_2|^2 - 2|B_3|^2)$
3	$-\frac{2}{15}\langle \overline{K}_1\rangle(|B_1|^2 - |B_2|^2)$
4	$\frac{4}{15}\langle \overline{K}_1\rangle\mathrm{Re}(B_1B_2^*)$
5	$\frac{2}{3}\langle \overline{K}_3\rangle\mathrm{Re}(B_1B_3^*) - \frac{2}{3}\langle \overline{K}_2\rangle\mathrm{Re}(B_2B_4^*)$
6	$\frac{2}{3}\langle \overline{K}_3\rangle\mathrm{Re}(B_2B_3^*) + \frac{2}{3}\langle \overline{K}_2\rangle\mathrm{Re}(B_1B_4^*)$
7	$\frac{2}{3}\langle \overline{K}_3\rangle\mathrm{Im}(B_1B_2^*) + \frac{2}{3}\langle \overline{K}_2\rangle\mathrm{Im}(B_3B_4^*)$
8	$\frac{4}{15}\langle \overline{K}_1\rangle\mathrm{Im}(B_1B_3^*)$
9	$-\frac{4}{15}\langle \overline{K}_1\rangle\mathrm{Im}(B_2B_3^*)$

various weighted differential widths are shown in Table II. The only weighted differential widths that include NP contributions are those with $i = 1, 5, 6,$ and 7. Therefore, the remaining observables are clearly CP even.

IV. OBSERVABLES

Since we are assuming that CP is violated via the pseudoscalar coupling, the τ^- and τ^+ distributions are not expected to be identical. There are in principle two ways to proceed. The first is to analyze the observables in Table II twice, once for the τ^- decay and once for the τ^+ decay. Another possibility is to perform an analysis separately for the *sum* and the *difference* of the distributions. We will follow the latter approach, since it has the advantage that the difference between the τ^- and τ^+ distributions is sensitive to the presence of CP violation. We define then the distributions

$$\frac{d\Gamma_i^\pm}{dQ^2ds_1ds_2} \equiv \frac{1}{2}\left(\frac{d\Gamma_i}{dQ^2ds_1ds_2} \pm \frac{d\overline{\Gamma}_i}{dQ^2ds_1ds_2}\right), \quad (14)$$

where $d\overline{\Gamma}_i/dQ^2ds_1ds_2$ is obtained from $d\Gamma_i/dQ^2ds_1ds_2$ by the replacement $B_4 \to \overline{B}_4$ (or, equivalently, $\eta_P \to \eta_P^*$); see Eqs. (11) and (12). We note that the quantities $d\Gamma_i^+/dQ^2ds_1ds_2$ and $d\Gamma_i^-/dQ^2ds_1ds_2$ are, by construction, CP even and CP odd, respectively. As was noted above, the only nonvanishing CP odd distributions are those with $i = 1, 5, 6,$ and 7, because the remaining weighted differential widths do not include NP contributions (i.e., they are independent of B_4).

Let us first consider the distributions with $i = 1$. After projection onto Q^2, s_1 or s_2, the CP-even distribution with $i = 1$ gives the CP-average of the invariant mass distributions, which are the distributions that are usually studied in experimental analyses [10,16]. The corresponding expression is obtained from Table II,

$$\frac{d\Gamma_1^+}{dQ^2ds_1ds_2} = A(Q^2)\left(\frac{2}{3}\langle K_1\rangle + \langle K_2\rangle\right)(|B_1|^2 + |B_2|^2 + |B_3|^2)$$
$$+ \frac{\langle K_2\rangle}{2}(|B_4|^2 + |\overline{B}_4|^2). \quad (15)$$

The CP-odd distribution with $i = 1$ is given by

$$\frac{d\Gamma_1^-}{dQ^2ds_1ds_2} = A(Q^2)\frac{\langle K_2\rangle}{2}(|B_4|^2 - |\overline{B}_4|^2)$$
$$= 2A(Q^2)\langle K_2\rangle\frac{Q^2}{m_\tau}|F_4f_H\eta_P|\sin(\delta_4 - \delta_H)\sin(\phi_H), \quad (16)$$

where δ_4 and δ_H denote the strong phases arising from the SM scalar form factor F_4 and the pseudoscalar form factor f_H, respectively, and ϕ_H is the weak phase present in η_P. The above expression is related to the well-known partial rate asymmetry. As was noted in Ref. [9], the partial rate asymmetry is expected to be doubly suppressed due to the generally assumed smallness of F_4 and η_P. Expressions for the remaining nonzero CP-even and CP-odd weighted partial differential widths may be found in Table III, where we have made use of the following definitions:

$$B_4^{(+)} \equiv \frac{1}{2}(B_4 + \overline{B}_4) = \sqrt{Q^2}\left[F_4 + \frac{f_H}{m_\tau}\mathrm{Re}(\eta_P)\right] \quad (17)$$

$$B_4^{(-)} \equiv \frac{1}{2}(B_4 - \overline{B}_4) = \frac{\sqrt{Q^2}if_H}{m_\tau}\mathrm{Im}(\eta_P). \quad (18)$$

Interestingly, from the definitions in Eqs. (17) and (18) and the results in Table III, we note that it does not seem to be possible to extract F_4 (by itself) from the data when $\phi_H \neq \pm\pi/2$. In other words, there will always be an

TABLE III. CP-even ("+") and CP-odd ("−") weighted partial widths. Several of the CP-odd weighted partial widths are zero; these have been omitted.

$i(\pm)$	$(d\Gamma_i^\pm/dQ^2ds_1ds_2)/A(Q^2)$
2(+)	$\frac{2}{15}\langle \overline{K}_1\rangle(|B_1|^2 + |B_2|^2 - 2|B_3|^2)$
3(+)	$-\frac{2}{15}\langle \overline{K}_1\rangle(|B_1|^2 - |B_2|^2)$
4(+)	$\frac{4}{15}\langle \overline{K}_1\rangle\mathrm{Re}(B_1B_2^*)$
5(+)	$\frac{2}{3}\langle \overline{K}_3\rangle\mathrm{Re}(B_1B_3^*) - \frac{2}{3}\langle \overline{K}_2\rangle\mathrm{Re}(B_2^*B_4^{(+)})$
6(+)	$\frac{2}{3}\langle \overline{K}_3\rangle\mathrm{Re}(B_2B_3^*) + \frac{2}{3}\langle \overline{K}_2\rangle\mathrm{Re}(B_1^*B_4^{(+)})$
7(+)	$\frac{2}{3}\langle \overline{K}_3\rangle\mathrm{Im}(B_1B_2^*) - \frac{2}{3}\langle \overline{K}_2\rangle\mathrm{Im}(B_3^*B_4^{(+)})$
8(+)	$\frac{4}{15}\langle \overline{K}_1\rangle\mathrm{Im}(B_1B_3^*)$
9(+)	$-\frac{4}{15}\langle \overline{K}_1\rangle\mathrm{Im}(B_2B_3^*)$
5(−)	$-\frac{2}{3}\langle \overline{K}_2\rangle\mathrm{Re}(B_2^*B_4^{(-)})$
6(−)	$\frac{2}{3}\langle \overline{K}_2\rangle\mathrm{Re}(B_1^*B_4^{(-)})$
7(−)	$-\frac{2}{3}\langle \overline{K}_2\rangle\mathrm{Im}(B_3^*B_4^{(-)})$

admixture of $f_H \eta_P^{R,1}$ and it will not be possible to distinguish them. However, if the coupling η_P were purely imaginary, the factor $B_4^{(+)}$ would only depend on the scalar form factor F_4 and then the CP-even observables with $i = 5, 6,$ and 7 would be useful for determining $F_4^{R,I}$.

To study the observables presented above (Table III), we have made various assumptions that tend to simplify the analysis, in a manner similar to the approach that was followed in Ref. [9]. First of all, note that the SM scalar form factor F_4 is generally assumed to be small for $\tau \to K\pi\pi\nu_\tau$, since there are no pseudoscalar resonances that mediate this decay. Therefore, we will neglect this contribution by setting $F_4 = 0$. Furthermore, we will assume that f_H has a flat behavior over the phase space (no Q^2, s_1, and s_2 dependence) and does not contain strong phases. Thus, we set $f_H^I = 0$. Under these assumptions the $1(-)$ distribution is reduced to zero, as can be seen from Eq. (16), while the $1(+)$ distribution becomes equal to the usual (unweighted) differential width, as follows from Eqs. (11), (12), and (15). Finally, in order to simplify and separate the analysis of the CP-even and CP-odd observables, we perform the analysis with $\phi_H = \pi/2$. For this particular value, $B_4^{(+)} = 0$, and the NP contribution is removed from the CP-even observables [see Eqs. (15) and (17), as well as Table III]. To set an input value for the quantity $|f_H \eta_P|$, we follow the approach adopted in Ref. [9], where it is assumed that the NP contribution to the width is hidden in the experimental uncertainty of the branching ratio. As shown there, the experimental uncertainty is saturated for $|f_H \eta_P| \simeq 17.9$. Thus, we take this value as a reference input. A few comments are in order at this point:

(1) As is noted in Ref. [9], one way to obtain an estimate of the order of magnitude of f_H is to compute F_4 within the context of chiral perturbation theory (see Ref. [15]) and then to relate f_H to F_4 via the quark equations of motion. The latter step yields $f_H \sim Q^2 F_4/m_s$. A numerical study along these lines, with kinematical variables sampled appropriately over the relevant phase space, shows that $\langle|f_H|\rangle \sim 14$, with 76% of the values falling within the range 7–21. Regarding the phase of f_H, one finds $\langle\arg(f_H)\rangle \simeq 0.97\pi$, so that $|\langle\mathrm{Im}(f_H)\rangle| \ll |\langle\mathrm{Re}(f_H)\rangle|$. Thus, it appears to be reasonable to assume that f_H is real.

(2) The NP parameter $|\eta_P|$ should scale as m_W^2/M^2 due to the charged scalar propagator, with m_W and M being the W and charged scalar masses, respectively. If the charged scalar has electroweak couplings, it would be reasonable to assume that η_P has a magnitude not exceeding unity.

(3) Combining the estimates from the above two comments, we obtain $|f_H \eta_P| \sim 14$, which is similar to our reference value $|f_H \eta_P| = 17.9$. As pointed out in Ref. [9], however, this estimate may well have large uncertainties due to the use of the quark equations of motion; a more realistic assumption would probably be to take $|f_H \eta_P|$ to be in the range 1–10.

(4) The decay channel $\tau^- \to K^- \nu_\tau$ also involves the pseudoscalar coupling η_P, so that this process can in principle be used to constrain the NP contribution to $\tau \to K\pi\pi\nu_\tau$. It turns out, however, that the constraints derived from $\tau^- \to K^- \nu_\tau$ are very sensitive to the values used for the strange quark mass and its uncertainty. By performing a crude estimate that takes into account the uncertainties of the K^- decay constant, f_{K^-}, and makes use of the quark equations of motion, we obtain the constraint $|\eta_P^I| < 0.364$ (recall our assumption that $\phi_H = \pi/2$). We note that this bound was derived by using the value $m_s = 0.095$ GeV. On the other hand, if the quark mass is replaced by the meson mass, one finds $|\eta_P^I| < 1.878$. By combining these constraints with the assumption that $1 < |f_H| < 10$, we obtain two different bounds, namely $|f_H \eta_P^I| < 3.64$ and $|f_H \eta_P^I| < 18.78$. Therefore, the constraints provided by the decay channel $\tau^- \to K^- \nu_\tau$ are not conclusive enough to discard our input value.

In much of the analysis that follows, we set $|f_H \eta_P| = 17.9$. With the above comments in mind, however, we also include some results for $f_H \eta_P = 1.79 e^{i\pi/4}$ in Sec. VI.

V. PARAMETRIZATION OF FORM FACTORS

We now introduce the parametrization of the form factors $F_1 - F_3$ appearing in the definitions of the quantities $B_1 - B_3$ in the expression for the differential width [see Eqs. (5) and (8)–(10)]. We write the form factors in terms of various Breit–Wigner functions in the following manner:

$$F_1(Q^2, s_1, s_2)$$
$$= -\frac{2N}{3F_\pi}[C \cdot BW_{1270}(Q^2) + D \cdot BW_{1400}(Q^2)]BW_{K^*}(s_2) \tag{19}$$

$$F_2(Q^2, s_1, s_2)$$
$$= -\frac{N}{\sqrt{3}F_\pi}[A \cdot BW_{1270}(Q^2) + B \cdot BW_{1400}(Q^2)]T_\rho^{(1)}(s_1) \tag{20}$$

$$F_3(Q^2, s_1, s_2)$$
$$= \frac{N_3}{2\sqrt{2}\pi^2 F_\pi^3} BW_{K^*}(Q^2)\left[\frac{T_\rho^{(1)}(s_1) + \alpha BW_{K^*}(s_2)}{1 + \alpha}\right]. \tag{21}$$

---

[1]From now on, we will use the superscripts R and I to denote the real and imaginary parts of a quantity, respectively.

The normalized Breit–Wigner propagators for the $K_1(1270)$ and the $K_1(1400)$ appearing in the axial vector form factors F_1 and F_2 are assumed to be [10]

$$BW_{K_1}(Q^2) = \frac{-m_{K_1}^2 + im_{K_1}\Gamma_{K_1}}{Q^2 - m_{K_1}^2 + im_{K_1}\Gamma_{K_1}}, \qquad (22)$$

where m_{K_1} and Γ_{K_1} denote the mass and width for the corresponding K_1 state. The Breit–Wigner propagators for the K^* and ρ are taken to have energy-dependent widths (see Refs. [10,17]),

$$BW_R(s) = \frac{-m_R^2}{s - m_R^2 + i\sqrt{s}\Gamma_R(s)}, \qquad (23)$$

with

$$\Gamma_R(s) = \Gamma_R \frac{m_R^2}{s}\left(\frac{p}{p_R}\right)^3, \qquad (24)$$

where

$$p = \frac{1}{2\sqrt{s}}\sqrt{[s - (m_1 + m_2)^2][s - (m_1 - m_2)^2]} \qquad (25)$$

$$p_R = \frac{1}{2m_R}\sqrt{[m_R^2 - (m_1 + m_2)^2][m_R^2 - (m_1 - m_2)^2]}. \qquad (26)$$

In the above expressions, the decay of the resonance R to two particles with masses m_1 and m_2 is assumed. For the K^*, a single resonance with an energy-dependent width is assumed, while the expression for the ρ includes two different resonances:

$$T_\rho^{(1)}(s_1) = \frac{BW_\rho(s_1) + \beta BW_{\rho'}(s_1)}{1 + \beta}. \qquad (27)$$

To fix the reference values for the parameters $A - D$ in Eqs. (19) and (20), we follow Ref. [10], where constraints arising from the tabulated branching fractions of the K_1 resonances are imposed. Regarding the parameters N and N_3 that regulate the contributions coming from the axial and anomalous form factors, respectively, we apply the criteria proposed in Ref. [9], in which 5% of the $\tau \to K\pi\pi\nu_\tau$ width is ascribed to the F_3 term and the remaining 95% to the F_1 and F_2 terms. For this computation, we have used the value of the branching ratio $\mathcal{B}(\tau \to K\pi\pi\nu_\tau)$ obtained in Ref. [18], which is the most precise one at present (see Refs. [16,19]). All the reference values related to the form factors $F_1 - F_3$ used in our analysis are listed in Table IV. Among them, those corresponding to the form factors F_1 and F_2 are based on Ref. [10]. We note that a more recent and precise value for the mass and the width of the $K_1(1270)$ resonance obtained in Ref. [20] from a signal-region fit for the channel $B^+ \to J/\psi K^+\pi^+\pi^-$ is still in

TABLE IV. Input values for the parameters entering in the form factors $F_1 - F_3$. The up table (a) lists the dimensionless parameters, while the down table (b) shows the masses and widths of the various resonances, along with the pion decay constant (F_π).

Parameter	Value
(a)	
α	−0.2
β	−0.145
A	0.944
B	0
C	0.195
D	0.266
N	1.4088
N_3	1.4696
(b)	
F_π	93.3 MeV
m_{1270}	1.254 GeV
Γ_{1270}	0.26 GeV
m_{1400}	1.463 GeV
Γ_{1400}	0.30 GeV
m_{K^*}	0.892 GeV
Γ_{K^*}	0.050 GeV
m_ρ	0.773 GeV
Γ_ρ	0.145 GeV
$m_{\rho'}$	1.370 GeV
$\Gamma_{\rho'}$	0.510 GeV

agreement with the input value used here. For the form factor F_3, we follow Ref. [15], whereas for the ρ and ρ' resonances, the input values are guided by Refs. [21,22].

VI. ANALYSIS

To study the proposed observables, we have performed two different analyses. In the first we have tested the SM hypothesis. In this case there are no CP-violating effects present in this decay, and hence the CP-odd observables in Table III are zero. In the second analysis, we have performed various fits of the distributions arising from all of the observables in Table III. Both analyses have been implemented by using our own Monte Carlo (MC) generator to simulate several sets of events with different sizes. The main goal of these two analyses is to estimate the number of events needed to detect the presence of NP (in the case of the SM test) and to extract the NP coupling (in the case of the fit to the CP-odd observables). Furthermore, the study of the CP-even observables aims to extract information about the resonant structure of the decay and, in particular, of the anomalous Wess-Zumino contribution.

We have focused our analysis on a scenario in which the NP parameter is assumed to be hidden in the experimental uncertainty of the branching ratio. Hence, as mentioned
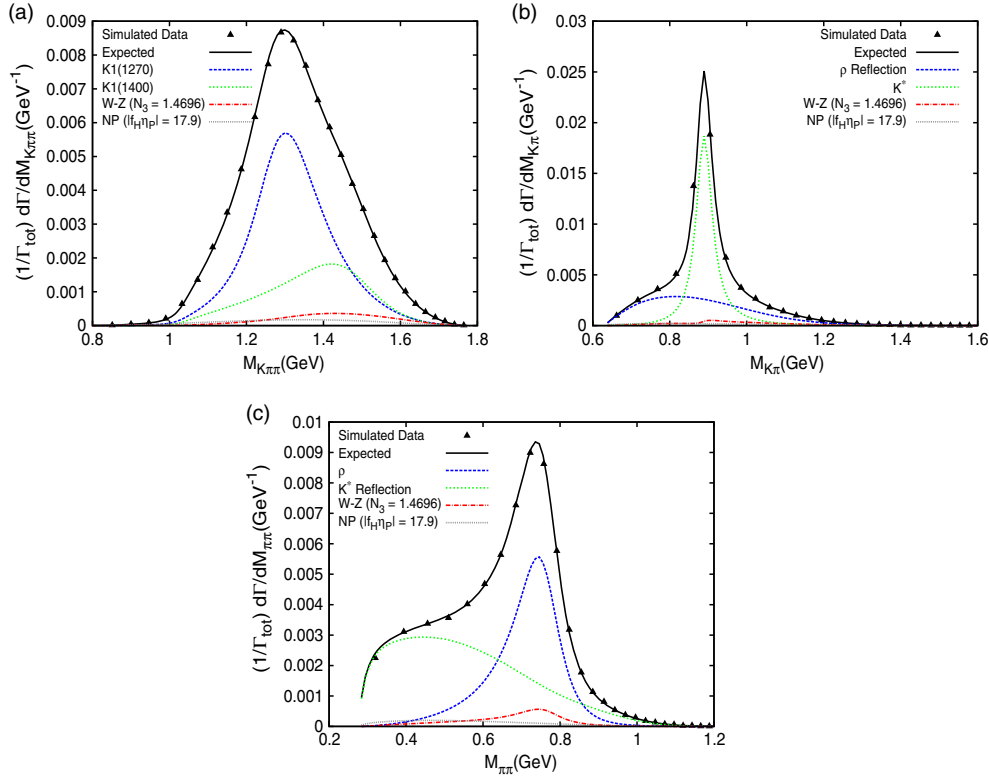
FIG. 1 (color online).   Plots of the differential widths $d\Gamma/dM$, including the different contributions from the decay chains along with the simulated data points obtained by using our MC generator. The $|f_H\eta_P|$ curve displays the NP contribution.

above, we have set the input value for the NP contribution to be $17.9e^{i\pi/2}$. To test the usefulness of the proposed observables when the NP contribution is considerably reduced, we have also performed an analysis of the CP-odd observables in the case where $f_H\eta_P = 1.79e^{i\pi/4}$.

A. Monte Carlo simulation

To simulate the distribution in Eq. (5), we have constructed a Monte Carlo event generator by applying von Neumann's acceptance-rejection technique. Once a set of events has been generated that is consistent with the differential decay width, the different observables can be obtained by using suitable estimators. By employing our own event generator, we are able to include different contributions to the differential decay width and to choose their parametrization. Various sets of events have been generated for the decay $\tau^- \to K^-\pi^+\pi^-\nu_\tau$ and for its CP conjugate, $\tau^+ \to K^+\pi^+\pi^-\bar{\nu}_\tau$. The maximum number of events was taken to be 3×10^6 for the case in which the NP parameter $f_H\eta_P$ is equal to $17.9e^{i\pi/2}$ and 10^6 for the case with $f_H\eta_P = 1.79e^{i\pi/4}$. Although the total number of events in these simulations is beyond the scope of the B-factories, it can be regarded as realistic within the context of the upcoming super B-factories, which are expected to increase the design luminosity by approximately 2 orders of magnitude. In fact, the design luminosity at SuperKEKB

is 8×10^{35} cm^{-2} s^{-1}, and an integrated luminosity of 50 ab^{-1} is expected [23]. Guided by the analysis performed in Ref. [16] (which was based on data collected by the Belle detector at KEKB) and taking into account the expected integrated luminosity at SuperKEKB, we can estimate the expected number of $\tau^- \to K^-\pi^-\pi^+\nu_\tau$ events. A conservative estimate gives $\sim 5 \times 10^6$, which is above the maximum number of events we have simulated for the present analysis, 3×10^6.[2]

As was noted in Sec. IV, the pseudoscalar form factor has been assumed to be real, and the SM scalar contribution has been neglected; thus, we have taken $f_H^I = F_4 = 0$ as inputs for the MC simulation. The input values related to the form factors $F_1 - F_3$ are listed in Table IV. As a test of the consistency of our event generator, the usual differential width distributions have been extracted from a set of 1×10^5 simulated events. As can be seen from Fig. 1, the simulated distributions are in agreement with those obtained experimentally by the CLEO collaboration in Ref. [10] and also with the expected distributions based on numerical computations [9]. In addition to the contributions involving the form factors F_1 and F_2, the subdominant

---

[2]Even though the estimated number of events takes into account the possible backgrounds as well as the detector effects [23], these have not been considered during the present analysis.

TABLE V. P-values corresponding to the observables $5(-)$ and $7(-)$. The number of events considered is given in the first column.

$N_{\rm ev}/100,000$	$d\Gamma_5^-/dQ^2$	$d\Gamma_5^-/ds_1$	$d\Gamma_5^-/ds_2$	$d\Gamma_7^-/dQ^2$	$d\Gamma_7^-/ds_1$	$d\Gamma_7^-/ds_2$
			P-values			
5	0.933	0.754	0.175	0.0086	0.168	0.057
10	0.675	0.361	0.0018	0.00015	0.044	0.00013
15	0.198	0.062	0.000015	1.15×10^{-7}	0.00033	4.27×10^{-7}
20	0.286	0.055	2.73×10^{-7}	2.78×10^{-10}	8.14×10^{-6}	9.76×10^{-11}

contribution from the W-Z term and the possible NP contribution have been incorporated in the plots.

B. SM hypothesis test

The fact that the CP-odd observables $5(-), 6(-)$, and $7(-)$ are zero if the NP contribution is absent (i.e., if $f_H \eta_P = 0$) allows for a test of the SM hypothesis by performing a Pearson's χ^2-test. To perform this test, we calculate χ^2 for a particular observable $j(-)$ and then compute the quantity P_j, which is the probability that the hypothesis (the SM hypothesis in our case) would lead to a χ^2 value greater than the one actually obtained,

$$\chi_j^2 = \sum_{i=1}^{N_{\rm bins}} \left[\frac{d_x \Gamma_j^-(x_i)}{\sigma_i^{(j)}} \right]^2, \quad P_j = \int_{\chi_j^2}^{\infty} f(z; n_d) dz, \quad j = 5, 6, 7.$$

$$(28)$$

In the above expressions, $d_x \equiv d/dx$ with $x \equiv Q^2, s_1, s_2$, $N_{\rm bins}$ is the number of bins,[3] $f(z; n_d)$ is the χ^2 distribution for n_d degrees of freedom, and $\sigma_i^{(j)}$ denotes the statistical uncertainty in the ith bin for the observable $j(-)$ (see Appendix A). We remark that the values of the distributions in the numerator of the expression for χ_j^2 given in Eq. (28) are extracted from the simulations. It is worth noting that this test is based on the assumption that the SM contribution only includes strong phases and therefore the only source of CP violation for the decay is a weak phase present in the NP contribution. Hence, the test itself does not depend on the particular value of the NP parameter, even when its robustness actually does (as we will show later). Tables V and VI show results of the SM hypothesis test performed using the observables $d\Gamma_{5,6,7}^-/dx$, with different numbers of events, and taking $f_H \eta_P = 17.9 e^{i\pi/2}$. As shown in Table VI, the SM test for the observable $6(-)$ allows one to reject the SM hypothesis with as few as 10^5 events. This is not the case for the other CP-odd observables, which are not useful for rejecting the null hypothesis unless there are at least 5×10^5 events. In fact, one can use this χ^2 test to rank the various observables in terms of their

sensitivity to the NP contribution. As is demonstrated by the data in Tables V and VI, the most sensitive observable appears to be the Q^2 projection of $6(-)$, which yields a P-value of 2.4×10^{-4} for 10^5 events. Therefore, the CP-odd differential width $6(-)$ (mainly its Q^2 projection) provides a suitable observable for rejecting the SM, since in the SM no CP violation effect is expected for this decay. To analyze the robustness of the test, we repeat the procedure with a sample of 10^6 events for the scenario in which $f_H \eta_P = 1.79 e^{i\pi/4}$. In this case the test seems to loose its capability of rejection, even for the observable $6(-)$ (see Table VII). The tiny NP contribution in this case makes all three CP-odd observables compatible with zero, at least for 10^6 events. This reveals that a larger set of events ($> 1 \times 10^6$) is needed for these observables to be useful when the NP contribution is this small. However, this test can be regarded as an interesting possibility within the context of the upcoming super B-factories, for which a conservative estimate of the expected number of events for the mode $\tau^- \to K^- \pi^- \pi^+ \nu_\tau$ gives $\sim 5 \times 10^6$, as was already mentioned in Sec. VI A.

TABLE VI. P-values for the observable $6(-)$. The number of events is shown in the first column. Note that in this case fewer events were included in the simulations than were used in the previous table.

$N_{\rm ev}/100,000$	$d\Gamma_6^-/dQ^2$	$d\Gamma_6^-/ds_1$	$d\Gamma_6^-/ds_2$
		P-values	
1	0.000024	0.0076	0.013
2	1.27×10^{-14}	1.05×10^{-7}	1.25×10^{-6}
3	$<10^{-17}$	6.66×10^{-16}	3.55×10^{-15}
4	$<10^{-17}$	$<10^{-17}$	$<10^{-17}$

TABLE VII. P-values corresponding to the observable $6(-)$ for a NP contribution with $f_H \eta_P = 1.79 e^{i\pi/4}$.

$N_{\rm ev}/100,000$	$d\Gamma_6^-/dQ^2$	$d\Gamma_6^-/ds_1$	$d\Gamma_6^-/ds_2$
		P-values	
10	0.53	0.93	0.99

---

[3]For the entire analysis, we have used the conservative number of 20 bins (see Ref. [16]).

C. Fitting procedure

We have performed several fits of the one-dimensional distributions resulting from the projections of the observables listed in Table III onto Q^2, s_1, and s_2. Only the parameters appearing linearly in the expressions for the form factors F_1 and F_2, namely A, B, C, and D, along with the NP parameter, $f_H\eta_P$, have been taken into account as possible fit parameters, although we have also tested the possibility of recovering N_3 (which provides information regarding the Wess-Zumino contribution) from the fits.[4] To construct the fitting function needed to apply the least-squares method, we write each observable in terms of the parameters $\underline{\theta} = (A, B, C, D, N_3, f_H\eta_P^I)$[5] as

$$\frac{d\Gamma_i^\pm}{dQ^2 ds_1 ds_2} = \sum_j f_j^{i(\pm)}(Q^2, s_1, s_2)\zeta_j^{i(\pm)}(\underline{\theta}), \quad (29)$$

where the vectors $\zeta^{i(\pm)}$ depend on the parameters $\underline{\theta}$ and are listed in Table VIII. By projecting Eq. (29) onto $x \equiv Q^2, s_1$, or s_2, we obtain the corresponding expected value for the ith projected partial differential width evaluated for the kth bin of x:

$$\left(\frac{d\Gamma_i^\pm}{dx}\right)_{\text{bin } k} = \sum_j c_{kj}^{i(\pm)} \zeta_j^{i(\pm)}(\underline{\theta}). \quad (30)$$

The matrices $c^{i(\pm)}$ in the above expression have dimension $N_{\text{bins}} \times N_{\text{coeff}}^{i(\pm)}$, with N_{bins} being the number of bins in the x range and $N_{\text{coeff}}^{i(\pm)}$ being the number of functions required to express the observable $i(\pm)$ in terms of the parameters $\underline{\theta}$ appearing in Eq. (29). The different matrices $c^{i(\pm)}$ are obtained by numerical integration of the appropriate function $f_j^{i(\pm)}(Q^2, s_1, s_2)$. With the observables expressed as in Eq. (30), we proceed in general to minimize the quantity

$$\chi^2(\underline{\theta}) = \sum_{j=1}^{N_{\text{bins}}} \frac{(y_j^{\text{sim}} - y_j^{\text{exp}}(\underline{\theta}))^2}{\sigma_j^2}, \quad (31)$$

where the y_j^{sim} are the values for a given observable extracted from the simulations, the y_j^{exp} are the

---

[4]Although the chosen fitting procedure does not take the masses and widths of the resonances as free parameters (i.e., these parameters are set to their reference values), we have also performed the fits by varying the values for the main contributing resonances $K_1(1270)$ and $K_1(1400)$ within the uncertainties reported in Ref. [10]. We have observed that these shifts tend to worsen the fits, whereas the uncertainties do not change significantly.

[5]We note that the fitting procedure introduced in this section could also be applied for the case $\phi_H \neq \pi/2$ by including the parameter $f_H\eta_P^R$ in $\underline{\theta}$.

TABLE VIII. List of the vectors $\zeta^{i(\pm)}$ appearing in Eq. (30) expressed in terms of the parameters in $\underline{\theta}$.

$i(\pm)$	ζ
2(+)	$(C^2, D^2, CD, A^2, B^2, AB, AC, BC, AD, BD, N_3^2)$
3(+)	$(C^2, D^2, CD, A^2, B^2, AB, AC, BC, AD, BD)$
4(+)	$(C^2, D^2, CD, A^2, B^2, AB, AC, BC, AD, BD)$
5(+)	$(N_3 C, N_3 D, N_3 A, N_3 B)$
6(+)	$(N_3 C, N_3 D, N_3 A, N_3 B)$
7(+)	(CA, CB, DA, DB)
8(+)	$(N_3 C, N_3 D, N_3 A, N_3 B)$
9(+)	$(N_3 C, N_3 D, N_3 A, N_3 B)$
5(−)	$(f_H\eta_P^I C, f_H\eta_P^I D, f_H\eta_P^I A, f_H\eta_P^I B)$
6(−)	$(f_H\eta_P^I C, f_H\eta_P^I D, f_H\eta_P^I A, f_H\eta_P^I B)$
7(−)	$(f_H\eta_P^I N_3)$

corresponding expected values obtained by using the fitting function defined above, and the σ_j are the statistical uncertainties associated with the simulation process (see Appendix A). We note that different choices of the parameters in $\underline{\theta}$ with respect to which $\chi^2(\underline{\theta})$ is minimized have been tested. The various resulting fits will be described in the following sections.

D. Fit results

We present now the results obtained by fitting the CP-odd as well as the CP-even observables (see Table III). We consider these two sets of observables separately. In the case of the CP-odd observables, we regard the NP parameter $f_H\eta_P$ as the unique free parameter and fix the remaining parameters to their input values. In the case of the CP-even observables we focus on extracting information about the remaining parameters, A, B, C, D, and N_3, from our simulated data. This approach is facilitated by the assumptions mentioned in Sec. IV, namely that $F_4 = f_H^I = 0$ and $\phi_H = \pi/2$. Under these assumptions, the CP-even observables in Table III do not depend on the NP contribution, and hence the input value for the parameter $f_H\eta_P$ is not involved in the analysis of these observables.[6]

1. CP-odd observables

To recover the NP parameter $f_H\eta_P^I$ from the CP-odd observables, we perform a least-squares fit by fixing the parameters A, C, and D to their input values and setting the parameter B to zero. The results obtained for two data sets

---

[6]Note that $f_H\eta_P$ is involved in the CP-even observable "1(+)" which is not included in Table III. Note also that, in the more general case in which $\phi_H \neq \pi/2$, the CP-even observables 5,6, and 7 contain NP contributions, but these are added to the dominant SM contribution. By way of contrast, the NP contributions are dominant for the CP-odd observables in the sense that these observables are zero if $f_H\eta_P = 0$ (since there is no weak phase in F_4).

TABLE IX.   Best fit values for the parameter $f_H\eta_P^I$ obtained from the CP-odd observables with a set of 5×10^5 events. The input value for the NP parameter was set at $f_H\eta_P^I = 17.9$. The difference between the best fit value and the input value, $|\Delta(f_H\eta_P^I)| \equiv |\hat{f_H\eta_P^I} - f_H\eta_P^I|$, is included.

				$N_{ev} = 5 \times 10^5$				
$d\Gamma_i^-/dQ^2$	$\hat{f_H\eta_P^I}$	$|\Delta(f_H\eta_P^I)|$	$d\Gamma_i^-/ds_1$	$\hat{f_H\eta_P^I}$	$|\Delta(f_H\eta_P^I)|$	$d\Gamma_i^-/ds_2$	$\hat{f_H\eta_P^I}$	$|\Delta(f_H\eta_P^I)|$
5	28 ± 11	0.9σ	5	21 ± 8	0.4σ	5	19 ± 5	0.2σ
6	17 ± 1	0.9σ	6	18 ± 1	0.1σ	6	17 ± 1	0.9σ
7	20 ± 4	0.5σ	7	17 ± 4	0.2σ	7	19 ± 4	0.3σ

TABLE X.   Best fit values for the parameter $f_H\eta_P^I$ obtained from the CP-odd observables with a set of 3×10^6 simulated events. The difference $|\Delta(f_H\eta_P^I)| \equiv |\hat{f_H\eta_P^I} - f_H\eta_P^I|$ is included.

				$N_{ev} = 3 \times 10^6$				
$d\Gamma_i^-/dQ^2$	$\hat{f_H\eta_P^I}$	$|\Delta(f_H\eta_P^I)|$	$d\Gamma_i^-/ds_1$	$\hat{f_H\eta_P^I}$	$|\Delta(f_H\eta_P^I)|$	$d\Gamma_i^-/ds_2$	$\hat{f_H\eta_P^I}$	$|\Delta(f_H\eta_P^I)|$
5	18 ± 5	0.02σ	5	22 ± 3	1.4σ	5	18 ± 2	0.05σ
6	17.6 ± 0.4	0.8σ	6	18.0 ± 0.5	0.2σ	6	17.4 ± 0.5	1.0σ
7	17 ± 2	0.5σ	7	15 ± 2	1.5σ	7	17 ± 2	0.5σ

TABLE XI.   Best fit values for the parameter $f_H\eta_P^I$ obtained from the observable $6(-)$ by using a set of 10^6 simulated events with an input value $f_H\eta_P = 1.79e^{i\pi/4}$ (so that $f_H\eta_P^I \simeq 1.27$).

				$N_{ev} = 1 \times 10^6$				
$d\Gamma_i^-/dQ^2$	$\hat{f_H\eta_P^I}$	$|\Delta(f_H\eta_P^I)|$	$d\Gamma_i^-/ds_1$	$\hat{f_H\eta_P^I}$	$|\Delta(f_H\eta_P^I)|$	$d\Gamma_i^-/ds_2$	$\hat{f_H\eta_P^I}$	$|\Delta(f_H\eta_P^I)|$
6	1.9 ± 0.6	1.1σ	6	1.8 ± 0.8	0.7σ	6	1.7 ± 0.8	0.5σ

(with different numbers of events) for the case $f_H\eta_P^I = 17.9$ are displayed in Tables IX and X.[7] The best fit value for $f_H\eta_P^I$ is more than 2.5σ away from zero for all of the CP-odd observables and is more compatible with the input value than with zero. Moreover, this is the case even when the number of events in the simulation is 5×10^5. As was the case for the SM test proposed in the previous section, the observable $6(-)$ appears to be more precise than the other CP-odd observables (judging by the smaller statistical uncertainty that it yields for the estimated parameter). As can be seen from the comparison between Tables IX and X, the statistical uncertainties are reduced by approximately 50% when the number of events in the simulation is increased from 5×10^5 to 3×10^6. We have also performed a least-squares fit using the set of 10^6 events with $f_H\eta_P = 1.79e^{i\pi/4}$. In this case the best values obtained from the fit to the observables $5(-)$ and $7(-)$ become compatible with zero and have large statistical uncertainties, whereas the observable $6(-)$ is still the most precise

one, giving best fit values that are more than 2σ away from zero and that recover the input value $f_H\eta_P^I = 1.79 \sin(\pi/4) \simeq 1.27$ even though the uncertainties are larger than those we obtain with $f_H\eta_P = 17.9e^{i\pi/2}$ using a set of 10^6 events.[8] The results for the three projections of the observable $6(-)$ are shown in Table XI.

Both the results obtained from the least-squares fit and the SM test indicate the utility of using the observable $6(-)$ as a tool for investigating CP-odd NP effects. On the one hand, the SM test shows this observable's power to reject the SM hypothesis if there is actually a CP-violating contribution; on the other hand, the least-squares fit demonstrates how this observable can be used to recover the input value of the NP parameter. It is interesting to consider why the $6(-)$ observable is so much more sensitive to CP violation than are the other two CP-odd observables that we have considered. This sensitivity arises from the dependence of the CP-odd observables on the quantities B_i. As is evident in Table III, the $7(-)$ observable is doubly suppressed due to the smallness

---

[7]In the tables in this and the next sections, the difference between the best fit value and the input value for each observable is given in units of its respective statistical uncertainty, although we use the same symbol σ everywhere.

[8]For the case with $f_H\eta_P = 17.9e^{i\pi/2}$ we only display results obtained using 5×10^5 and 3×10^6 events, although we have also performed similar fits using sets of events of different sizes.

of the W-Z and the NP contributions. Similarly, comparison of the $5(-)$ and $6(-)$ observables indicates that the latter exhibits a larger magnitude (and hence greater sensitivity to NP) because it depends on the quantity B_1, whereas the former depends on B_2; numerical study has shown that the magnitude of B_1 tends to be larger than that of B_2 within the allowed ranges of Q^2, s_1, and s_2.

The above results are based on the assumption that f_H has no Q^2, s_1, or s_2 dependence. It is important to note, however, that a nontrivial dependence on the kinematical variables could appear due to the presence of final state interactions. The functional form of f_H is unknown at present. Having said this, it is instructive to adopt a simple functional form for f_H in order to test how the $6(-)$ distributions are modified. For the purpose of illustration, let us reconsider the expression for f_H derived from the quark equations of motion, $f_H \sim (Q^2/m_s)F_4$, where F_4 is assumed to be a constant. To set a reference value for $|F_4|$, the expression derived in Ref. [15] within the context of chiral perturbation theory has been used. A numerical analysis similar to that discussed in Sec. IV gives $\langle|F_4|\rangle \sim 0.54 \text{ GeV}^{-1}$ and $\mathcal{O}(\langle\text{Im}(F_4)\rangle) < \mathcal{O}(\langle\text{Re}(F_4)\rangle)$. We set $F_4 = 0.54 \text{ GeV}^{-1}$ and add a normalization factor in the expression for f_H, $\mathcal{N}$, so that the experimental uncertainty of the branching ratio is again saturated by the NP

contribution. By taking $\phi_H = \pi/2$ we find the value $\mathcal{N}|\eta_P| = 1.71$. Hence, $|f_H\eta_P| = \mathcal{N}(Q^2/m_s)F_4|\eta_P| = 1.71 \times 0.54 \text{ GeV}^{-1}(Q^2/m_s) = 0.92 \text{ GeV}^{-1}(Q^2/m_s)$. Figure 2 shows plots of the $6(-)$ distributions for the case $f_H\eta_P^I = 17.9$ (blue solid line) along with the specific case presented above in which f_H depends linearly on Q^2 (red dashed line). These distributions have been obtained numerically and normalized to the total width of the τ (Γ_{tot}).

As can be seen from the plots, the $6(-)$ distributions arising from the two approaches are comparable. On the one hand, the order of magnitude of each projection remains the same in both cases. On the other hand, the maxima of the distributions do not change significantly from one approach to the other. Based on these facts, it would be reasonable to expect that the number of events needed for recovering the NP parameter from the $6(-)$ distributions in the case $|f_H\eta_P| = 17.9$ would also be enough for the case $|f_H\eta_P| \propto Q^2$. In this sense, the presence of a linear Q^2 dependence in f_H should not spoil the sensitivity of the $6(-)$ distributions to the NP contribution with respect to the case in which $|f_H|$ is assumed to be a flat function. Hence, this specific case shows that the proposed observables could be useful even when there is a non-trivial dependence of $|f_H|$ on Q^2, s_1 and s_2.
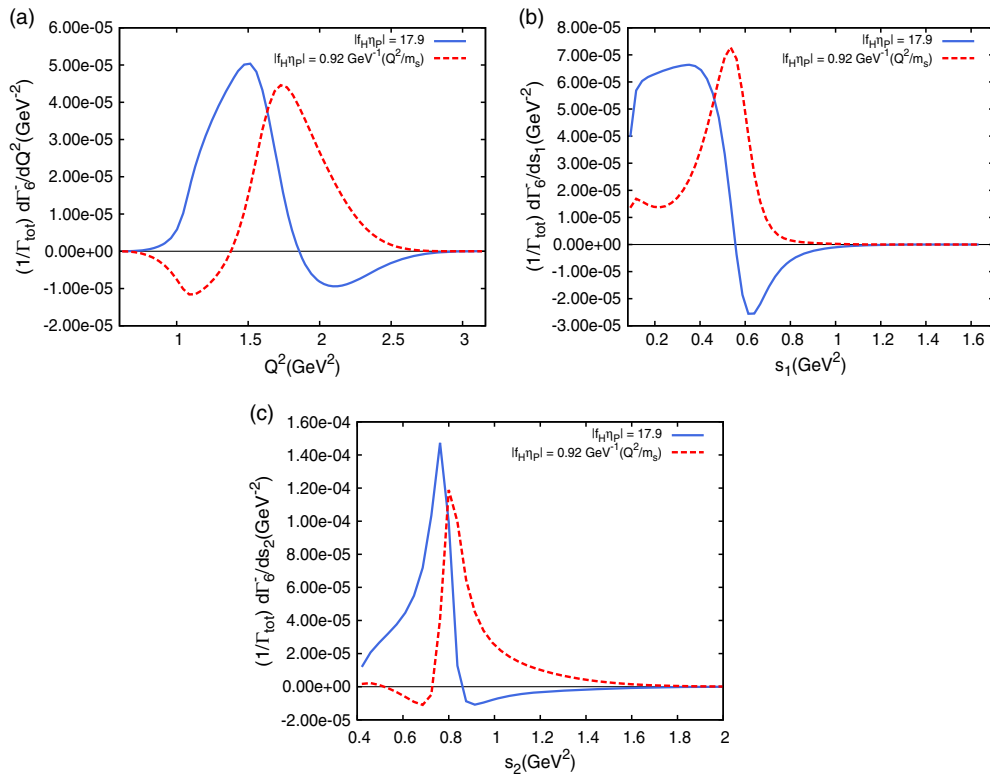

FIG. 2 (color online).   Plots of the distributions obtained from the observable $6(-)$ for $|f_H\eta_P| = 17.9$ (blue solid line) and $|f_H\eta_P| = 0.92 \text{ GeV}^{-1}(Q^2/m_s)$ (red dashed line). In the panels (a), (b), and (c), the projections onto Q^2, s_1, and s_2 are displayed, respectively. The distributions are normalized to the total width of the τ.

TABLE XII.   Fit results for the parameter A obtained from the CP-even observables $2(+) - 7(+)$ using a sample of 3×10^6 simulated events. The input value for the simulation was taken to be $A = 0.944$. The difference $|\Delta A| \equiv |\hat{A} - A|$ is also displayed.

				$N_{\text{ev}} = 3 \times 10^6$				
$d\Gamma_i^+/dQ^2$	$\hat{A}$	$|\Delta A|$	$d\Gamma_i^+/ds_1$	$\hat{A}$	$|\Delta A|$	$d\Gamma_i^+/ds_2$	$\hat{A}$	$|\Delta A|$
2	0.95 ± 0.01	0.6σ	2	0.94 ± 0.01	0.4σ	2	0.94 ± 0.02	0.2σ
3	0.92 ± 0.01	2.4σ	3	0.91 ± 0.01	3.4σ	3	0.91 ± 0.02	1.7σ
4	0.93 ± 0.02	0.7σ	4	0.94 ± 0.01	0.4σ	4	0.94 ± 0.02	0.2σ
5	0.949 ± 0.008	0.6σ	5	0.947 ± 0.006	0.6σ	5	0.942 ± 0.006	0.3σ
6	0.91 ± 0.03	1.1σ	6	0.92 ± 0.02	1.2σ	6	0.92 ± 0.02	1.2σ
7	0.94 ± 0.01	0.4σ	7	0.942 ± 0.008	0.3σ	7	0.948 ± 0.005	0.8σ

2. CP-even observables

In this section we focus on CP-even observables. We will discuss the results arising from the observables $2(+) - 9(+)$ and then, separately, those arising from the $1(+)$ distribution, due to its preferential treatment in previous analyses [10,16].

To test the power of the method, we first performed a fit with the parameters A, C, D, and N_3 unconstrained and B set to zero. In this case, we observe that the correlation between the parameters, as well as the standard deviations, are very large and the outputs of the fit for the different parameters are far away from the input values. To address these issues, we have adopted a modified fit procedure, in which the parameters C and D are constrained by the branching fractions into the $K^*\pi$ final state from the $K_1(1270)$ and $K_1(1400)$, respectively (see Ref. [10]). In addition, we keep the parameters B and N_3 fixed to their input values, $B = 0$ and $N_3 = 1.4696$, respectively. Accordingly, we have minimized the distributions only with respect to the parameter A. The results of the fit for 3×10^6 events are tabulated in Table XII. Before we discuss the results in Table XII, we note that the $8(+)$ and $9(+)$ distributions extracted from the set of 3×10^6 simulated events are consistent with zero to within their statistical uncertainties [which are determined using Eq. (A2)]. As a result, no conclusive information can be obtained from these observables with this number of events. For this reason we do not include results from these observables in the table. Turning now to the observables $2(+) - 7(+)$, we notice that for these observables the input value is recovered in all cases with uncertainties smaller than 3%; furthermore, the three projections of $5(+)$ and the $s_{1,2}$ projections of $7(+)$ are the most precise, with uncertainties smaller than 1%.

We turn now to a consideration of the observable $1(+)$. All of the projections of this observable are positive distributions that are more than two orders of magnitude larger than those arising from the other CP-even observables. Since the absolute statistical uncertainties are similar for all of the CP-even distributions, the $1(+)$ distributions end up having considerably reduced relative statistical uncertainties compared to those for the other CP-even distributions. Therefore, we have analyzed this distribution in a different manner, allowing A, N_3, and $f_H\eta_P$ to float as free parameters. Although the best fit point obtained from the fit to the $1(+)$ distribution is in good agreement with the corresponding input values, and the standard deviations are smaller than those associated with the other observables, there are certain disadvantages in the use of this distribution for extracting the value of $f_H\eta_P$. First of all, it is important to note that the fact that the distribution appears to be sensitive to the NP contribution arises exclusively from the input value that we have used for the NP parameter. More precisely, as outlined above, the NP parameter has been set to a value such that it saturates the experimental uncertainty, which includes both statistical and systematic sources. This experimental uncertainty is higher than the uncertainty associated with extracting the distributions from the simulations, which is purely statistical. Moreover, the statistical uncertainty that we have used in our analysis is smaller than the statistical uncertainties in the experiments since we are using a larger number of events for our simulation. Therefore, in our analysis, the NP contribution exceeds the statistical uncertainties of the simulated $1(+)$ distribution, leading to a best fit value for $f_H\eta_P$ essentially incompatible with zero. This observation is supported by the fact that, when we carry out the same fit using the set of events simulated with $f_H\eta_P = 1.79e^{i\pi/4}$, we obtain a best fit value in agreement with zero. Moreover, the computation of the correlation matrix for both sets of events shows that there are significant correlations between the fit parameters. Furthermore, the least-squares function that we minimize exhibits several local minima that are not far enough from the global minimum to distinguish them if the precise input values are not known beforehand. It is worth noting that this sort of problem is absent when we fit the CP-odd observables in order to obtain the single NP parameter.[9] Lastly, note that under the assumptions used in this work one would not be able to extract any

---

[9]This could arise from the fact that, for the observable $1(+)$, the χ^2 is a quartic function of the input parameters, whereas for the CP-odd observables it is a quadratic function of the NP parameter.

TABLE XIII. Results for N_3 from fits to the $5(+)$ and $6(+)$ distributions with a set of 3×10^6 simulated events. The fit has been performed by fixing the parameters A, C, and D to their input values. The input value for N_3 was 1.4696.

				$N_{\rm ev} = 3 \times 10^6$				
$d\Gamma_i^+/dQ^2$	$\hat{N}_3$	$|\Delta N_3|$	$d\Gamma_i^+/ds_1$	$\hat{N}_3$	$|\Delta N_3|$	$d\Gamma_i^+/ds_2$	$\hat{N}_3$	$|\Delta N_3|$
5	1.45 ± 0.05	0.4σ	5	1.45 ± 0.05	0.4σ	5	1.49 ± 0.05	0.4σ
6	1.3 ± 0.2	0.9σ	6	1.5 ± 0.2	0.2σ	6	1.5 ± 0.2	0.2σ

information about the NP weak phase from the analysis of the $1(+)$ distribution because its dependence on the NP parameter enters as the squared modulus of B_4 and $\overline{B}_4$, which are proportional to $|\eta_P|$ under our assumption that $F_4 = 0$ [see Eqs. (11), (12), and (15)]. Even if $F_4 \neq 0$, the dependence on the NP parameter would be mixed in a complicated way with the dependence on the SM scalar form factor F_4, preventing their disentanglement. We remark that the inability to distinguish the NP contribution from the SM contribution is common to all the *CP*-even observables, while it is absent in the case of the *CP*-odd observables.

Several of the *CP*-even observables are in principle sensitive to the parameter N_3 (which fixes the contribution of the anomalous Wess-Zumino term). However, as was noted above, the $8(+)$ and $9(+)$ distributions are consistent with zero, even with the maximum number of events that we have simulated. This spoils the sensitivity of these observables to the parameter N_3. An alternative is to use the observables $5(+)$ and/or $6(+)$ with the parameters A, C, and D fixed to their input values. With these parameters fixed in this way, the $5(+)$ and $6(+)$ distributions depend only on N_3. Of course, when experimental data are used instead of simulated events, the input values will be unknown. In this case, one could use the other observables to estimate the parameter A first; then C and D could be obtained by applying constraints arising from the tabulated branching fractions of the K_1 resonances (see Eqs. (8)–(10) in Ref. [10]). The results for N_3 obtained from the $5(+)$ and $6(+)$ distributions are shown in Table XIII for a simulation using 3×10^6 events. Both observables allow one to recover the parameter N_3. The observable $5(+)$, however, is the more precise of the two; its uncertainties are smaller than 4%, while those associated with the $6(+)$ distribution are of order 15%. Hence,

the observable $5(+)$ appears to be the most appropriate observable for implementing the proposed strategy to extract information about the anomalous Wess-Zumino contribution.

We conclude this section by summarizing, in Table XIV, the main results obtained for the $6(-)$ observable. Of the various observables proposed in this work, the $6(-)$ distribution shows the most promise for detecting *CP*-odd NP effects in $\tau \to K\pi\nu_\tau$.

VII. $\tau \to K\pi\nu_\tau$ WITHIN THE ALIGNED 2HDM

So far we have analyzed the decay $\tau \to K\pi\nu_\tau$ in a model-independent framework, in which the NP effects are incorporated by adding the contribution of a charged scalar boson that couples to fermions in a "nonstandard" manner (i.e., the couplings are not suppressed by the masses of the light quarks [9]). In this section we consider the proposed analysis in the context of a particular model of NP. Many NP models extend the SM scalar sector by adding a second scalar doublet so that the scalar spectrum contains a charged boson. A particular example of such a model is the so-called aligned two-Higgs-doublet model [11]. In the A2HDM, an alignment between Yukawa coupling matrices leads to the elimination of the nondiagonal neutral couplings that would lead to tree-level flavor-changing neutral currents.

The Yukawa Lagrangian corresponding to the charged Higgs boson in the A2HDM can be written in terms of the fermion mass eigenstates as [11,12]

$$\mathcal{L}_Y^{H^\pm} = -\frac{\sqrt{2}}{v} H^+ \{\overline{u}[\varsigma_d V M_d \mathcal{P}_R - \varsigma_u M_u V \mathcal{P}_L]d + \varsigma_l \overline{\nu} M_l \mathcal{P}_R l\} + \text{H.c.}, \tag{32}$$

where $M_{u,d}$ are the diagonal mass matrices, V is the Cabibbo-Kobayashi-Maskawa (CKM) matrix, v is the Higgs vacuum expectation value, and $\mathcal{P}_{R,L} \equiv \frac{1 \pm \gamma_5}{2}$ are the chirality projection operators. The proportionality parameters $\varsigma_f (f = u, d, l)$ are arbitrary complex numbers and give rise to new sources of *CP* violation.

From Eq. (32) we see that within the A2HDM the effective couplings $g_L^{q_u q_d l}$ and $g_R^{q_u q_d l}$ appearing in the corresponding effective Hamiltonian are given by [11]

TABLE XIV. Main results for the $6(-)$ observable obtained in Sec. VI by using various sets of simulated events with $|f_H \eta_P| = 17.9$.

	SM hypothesis test		Least-squares fit	
Distribution	$N_{\rm ev}$	P-value	$N_{\rm ev}$	Fit value for $f_H \eta_P^l$
$d\Gamma_6^-/dQ^2$	10^5	0.000024	3×10^6	17.6 ± 0.4
$d\Gamma_6^-/ds_1$	10^5	0.0076	3×10^6	18.0 ± 0.5
$d\Gamma_6^-/ds_2$	10^5	0.013	3×10^6	17.4 ± 0.5

$$g_L^{q_u q_d l} = \varsigma_u \varsigma_l^* \frac{m_{q_u} m_l}{M_{H^\pm}^2}, \qquad g_R^{q_u q_d l} = -\varsigma_d \varsigma_l^* \frac{m_{q_d} m_l}{M_{H^\pm}^2}. \quad (33)$$

Moreover, given the three-family universality of the proportionality parameters ς_f, the following relations are satisfied:

$$\frac{g_L^{q_u q_d l}}{g_L^{q'_u q'_d l'}} = \frac{m_{q_u} m_l}{m_{q'_u} m_{l'}}, \qquad \frac{g_R^{q_u q_d l}}{g_R^{q'_u q'_d l'}} = \frac{m_{q_d} m_l}{m_{q'_d} m_{l'}}. \quad (34)$$

In our case, the relations between the couplings $\eta_{P,S}$ defined in Eq. (2) and those introduced in Eq. (33) are given by

$$\frac{\eta_S^* + \eta_P^*}{2} = g_L^{us\tau} \doteq \varsigma_u \varsigma_l^* \frac{m_u m_\tau}{M_{H^\pm}^2} \quad \text{and}$$

$$\frac{\eta_S^* - \eta_P^*}{2} = g_R^{us\tau} \doteq -\varsigma_d \varsigma_l^* \frac{m_s m_\tau}{M_{H^\pm}^2}, \quad (35)$$

where the last equalities hold only within the A2HDM. Owing to the m_u suppression, $g_L^{us\tau}$ can be neglected, and the relations in Eq. (35) reduce to

$$\eta_P = -g_R^{us\tau*} \doteq \varsigma_d^* \varsigma_l \frac{m_s m_\tau}{M_{H^\pm}^2}. \quad (36)$$

The above expression, along with the second relation in Eq. (34), implies that observables from other systems involving the couplings $g_R^{q_u q_d l}$ will provide constraints for the pseudoscalar coupling η_P, which can be used in turn to obtain predictions for the observables proposed in Sec. IV. In this case, the observables we have proposed could be useful for testing the A2HDM.

Let us now consider an example that will illustrate how outside constraints can be used to make testable predictions in $\tau \to K\pi\pi\nu_\tau$. In this example we will focus on the observable $6(-)$, which happens to be much more sensitive to CP violation than the other proposed observables, as was discussed in Sec. VI D 1. The phenomenology derived from the A2HDM has been studied extensively (see for example Refs. [11,13]). In particular, the constraints obtained by combining the information from various semileptonic and leptonic decays have been discussed in Refs. [11,12]. Hence, guided by Ref. [12], and assuming that $1 < |f_H| < 10$ and that $f_H^I = 0$, we derive the (model-dependent) constraints $-0.01 < f_H \eta_P^{R,I} < 0.01$. It should be noted that in this case we are considering an arbitrary weak phase ϕ_H, in contrast with our analysis in Sec. VI, in which the analysis was restricted to $\phi_H = \pi/2, \pi/4$. To test the A2HDM, the $6(-)$ distributions extracted from the data can be compared to the corresponding allowed region arising from the very restrictive bound mentioned above. Since we are using simulated events instead of experimental data, we will make use of the $6(-)$ distributions extracted from our simulations. In particular, we will use

the distributions associated with the NP parameter choice $f_H \eta_P = 1.79 e^{i\pi/4}$, instead of those associated with $f_H \eta_P = 17.9 e^{i\pi/2}$, since the former parameter choice is closer to the range obtained from the A2HDM. In addition, we note that this parameter choice is compatible with the constraints derived in a model-independent manner from the decay $\tau \to K\nu_\tau$ (assuming that $f_H^I = 0$ and that $1 < |f_H| < 10$), regardless of whether one uses the quark or meson mass to determine the bound. The projection onto s_2 of the observable $6(-)$ is displayed in Fig. 3 along with the prediction derived from the A2HDM. We consider only the s_2 projection because it tends to have the largest magnitude for this observable. Inspection of Fig. 3 reveals that the distribution lies outside the A2HDM prediction only in the third and fourth bins, with the deviations being smaller than 2σ and almost 1σ, respectively. However, as was already shown in Sec. VI D 1, when we perform a least-squares fit to this distribution with $f_H \eta_P^I$ as the unique free parameter, we obtain the value 1.7 ± 0.8 (see Table XI), which is more than 2σ away from the range allowed for this parameter within the A2HDM ($|f_H \eta_P^I| < 0.01$). Although such a deviation would cast doubt on the A2HDM in an experimental setting, it would not be enough to completely reject the model. Thus, for a NP parameter $f_H \eta_P^I$ two orders of magnitude above the range predicted by the A2HDM, more than 10^6 events would be needed for the observable $6(-)$ to be useful in probing this model. A similar observation holds for the case of the SM, since in that case the $6(-)$ distribution is simply zero and is thus contained within the range allowed for the A2HDM. In fact, the situation here is similar to the situation that was considered in Secs. VI B and VI D 1,
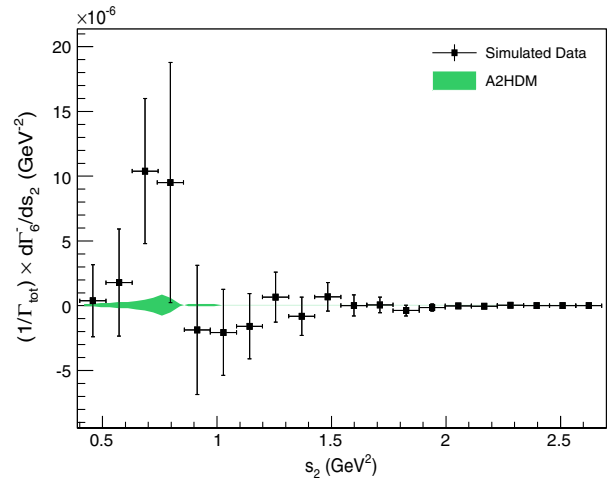

FIG. 3 (color online). Projection onto s_2 of the observable $6(-)$ extracted from a set of 10^6 events along with the corresponding allowed region within the A2HDM. The data in the simulation correspond to the NP parameter choice $f_H \eta_P = 1.79 e^{i\pi/4}$. Note that the plot of the allowed region assumes that the parameters associated with the form factors (A, B, etc.) have zero uncertainty.

where it was noted that more than 10^6 events were required to use the $6(-)$ distribution as a tool for distinguishing between the SM and a NP scenario with $|f_H \eta_P| = 1.79$.

Finally, we emphasize that the allowed region indicated in Fig. 3 assumes that the pseudoscalar form factor f_H is a constant function of the phase space variables and that its imaginary part is zero. To perform a more realistic study of the A2HDM within the context of the observables discussed in this work, these assumptions would need to be tested carefully. In Sec. VIII we comment on some possibilities for testing these assumptions.

VIII. TEST OF ASSUMPTIONS

As has been mentioned in previous sections, various assumptions have been made while performing the analysis in this work. Some of these assumptions could in principle be tested by using the proposed observables. In this section we describe how one could test two assumptions that have been made regarding the pseudoscalar form factor f_H, namely, that it is a flat function of Q^2, s_1, and s_2 and that it does not contain strong phases (i.e., that f_H^I is zero).

From the observables $5(-)$ and $6(-)$ in Table III, we have the relations

$$\frac{d\Gamma_5^-}{dQ^2 ds_1 ds_2} = \left(\frac{2}{3} A(Q^2) \langle \overline{K}_2 \rangle \frac{\sqrt{Q^2}}{m_\tau} B_2^R \right) f_H^I \eta_P^I$$
$$- \left(\frac{2}{3} A(Q^2) \langle \overline{K}_2 \rangle \frac{\sqrt{Q^2}}{m_\tau} B_2^I \right) f_H^R \eta_P^I \quad (37)$$

$$\frac{d\Gamma_6^-}{dQ^2 ds_1 ds_2} = -\left(\frac{2}{3} A(Q^2) \langle \overline{K}_2 \rangle \frac{\sqrt{Q^2}}{m_\tau} B_1^R \right) f_H^I \eta_P^I$$
$$+ \left(\frac{2}{3} A(Q^2) \langle \overline{K}_2 \rangle \frac{\sqrt{Q^2}}{m_\tau} B_1^I \right) f_H^R \eta_P^I, \quad (38)$$

where we recall that the quantities B_1, B_2, and $\langle \overline{K}_2 \rangle$ depend on the kinematical variables Q^2, s_1, and s_2. By projecting Eqs. (37) and (38) onto $x \equiv Q^2, s_1, s_2$, we can form a 2×2 matrix equation,

$$\begin{pmatrix} d\Gamma_5^-/dx \\ d\Gamma_6^-/dx \end{pmatrix} = \begin{pmatrix} a_1 & -b_1 \\ -a_2 & b_2 \end{pmatrix} \begin{pmatrix} f_H^I \eta_P^I \\ f_H^R \eta_P^I \end{pmatrix}, \quad (39)$$

where the quantities a_1 and b_1 are the projections onto x of the two functions appearing inside the parentheses in Eq. (37), while a_2 and b_2 arise from the two functions in Eq. (38). Of course, these quantities are functions of x. Also, we note that we need to assume that f_H has no dependence on the kinematical variables other than x in order to derive Eq. (39). By inverting Eq. (39), we obtain the relations

$$f_H^I \eta_P^I = \frac{1}{a_1 b_2 - a_2 b_1} \left(b_2 \frac{d\Gamma_5^-}{dx} + b_1 \frac{d\Gamma_6^-}{dx} \right) \quad (40)$$

$$f_H^R \eta_P^I = \frac{1}{a_1 b_2 - a_2 b_1} \left(a_2 \frac{d\Gamma_5^-}{dx} + a_1 \frac{d\Gamma_6^-}{dx} \right), \quad (41)$$

from which we find

$$\frac{f_H^I}{f_H^R} = \frac{b_2 d\Gamma_5^-/dx + b_1 d\Gamma_6^-/dx}{a_2 d\Gamma_5^-/dx + a_1 d\Gamma_6^-/dx}. \quad (42)$$

Since we are assuming that there is no Q^2, s_1, or s_2 dependence in f_H, the right-hand side of Eq. (40) as well as of Eq. (41) must be constant over the range of x. Therefore, by extracting the distributions $d_x \Gamma_{5,6}^-$ from the data and obtaining the quantities $a_{1,2}, b_{1,2}$ numerically for each bin in the x range, the assumption regarding the flatness of f_H (as a function of Q^2, s_1, and s_2) can be tested. On the other hand, under the assumption that f_H has no strong phase, the left-hand side of Eq. (42) vanishes, so that the significance of the deviations from zero of the quantity appearing on the right-hand side can be used to test this assumption.

Another possibility arises from the analysis of the zero-crossing points for the various distributions. Under the assumptions mentioned above, namely that $f_H^I = 0$ and that its functional dependence on the kinematical variables is flat, the zero-crossing points for the CP-odd distributions are independent of the value of the NP parameter $f_H \eta_P$. Thus, the numerical prediction of these zero-crossing points and the comparison with the distributions obtained from the data can also be used to test these two assumptions.[10] To illustrate this, let us consider the observable $6(-)$ (see Fig. 2). Projecting this distribution separately onto Q^2, s_1, and s_2 and performing a numerical computation of the corresponding zero-crossing points yields the values $Q^2 \sim 1.85609 \text{ GeV}^2$, $s_1 \sim 0.55633 \text{ GeV}^2$, and $s_2 \sim 0.85142 \text{ GeV}^2$, respectively. On the other hand, analysis of the distributions associated with a set of 3×10^6 events yields the values (see Fig. 4)

$$Q^2 = 1.86 \pm 0.04 \text{ GeV}^2, \qquad s_1 = 0.56 \pm 0.03 \text{ GeV}^2,$$
$$s_2 = 0.84 \pm 0.04 \text{ GeV}^2, \quad (43)$$

which are in good agreement with the expected values. Thus, with 3×10^6 events, it appears that one could use the zero-crossing points of the CP-odd distributions to test the assumptions regarding f_H that were noted above. With

---

[10]Here we are taking the parameters related to the resonance structure of the decay to be fixed to their input values. In fact, the position of the zero-crossing points depends not only on the two assumptions we are testing but also on these input values. In this sense, the analysis of the zero-crossing points could also be useful for studying these parameters.
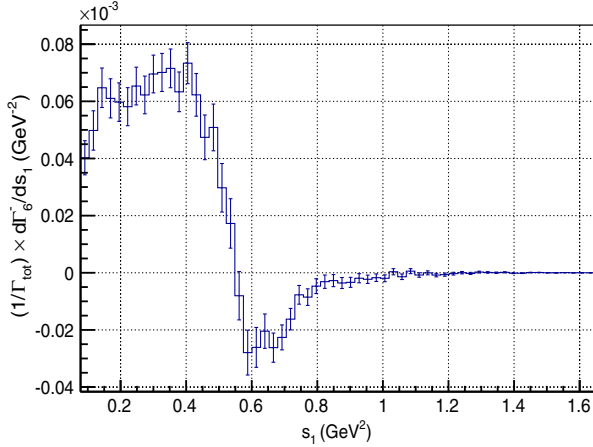
FIG. 4 (color online).   Projection onto s_1 of the observable $6(-)$, obtained by using a set of 3×10^6 simulated events. The zero-crossing point can be clearly extracted from the plot with an uncertainty given by the size of the bins ($s_1 = 0.56 \pm 0.03$ GeV^2).

fewer than 3×10^6 events, however, the zero-crossing point test would start to lose its effectiveness.

IX. CONCLUSIONS

In this paper we have proposed and tested various CP-even and CP-odd observables for the decay $\tau \to K\pi\nu_\tau$ by adding the contribution of a NP charged scalar to the corresponding amplitude within a model-independent approach. The various observables that we have proposed are defined in Eq. (14) (see also Tables I and III). These observables are distributions that have been partially integrated over phase space, using weighting functions to pick out various terms from the original expression for the differential width [see Eq. (5)]. The resulting distributions are functions of three invariant mass squared variables, Q^2, s_1, and s_2, and they depend on the NP contribution in different ways. Throughout much of the text, we have denoted the various distributions by "$i(\pm)$" ($i = 1, ..., 9$), where the "$\pm$" designation refers to whether the distribution is even ("$+$") or odd ("$-$") under CP. For the numerical analysis, we have used simulated events generated through our own event generator, with the maximum number of simulated events being 3×10^6.

Among the various observables that we have proposed, the $6(-)$ distribution is the most sensitive to the NP contribution. On the one hand, for a sizeable NP contribution ($|f_H\eta_P| \sim 17.9$), we have found that this observable is useful for testing the SM hypothesis, even for 1×10^5 events. On the other hand, the results of the fits show that this observable allows one to recover the NP parameter with the highest precision, with the uncertainties being $\lesssim 6\%$ and $\lesssim 3\%$ for 5×10^5 and 3×10^6 simulated events, respectively. More interestingly, the capability of the observable $6(-)$ to recover the NP parameter is not spoiled when the size of the NP contribution is reduced.

Regarding the CP-even observables that we study in this paper, we have found that the $5(+)$ distribution and the $s_{1,2}$ projections of the $7(+)$ distribution show the most promise for recovering the parameter A, which is related to the weight of the resonant contributions. Additionally, considering that the $8(+)$ and $9(+)$ distributions extracted from the set of 3×10^6 simulated events are consistent with zero to within their statistical uncertainties, we have shown that the observable $5(+)$ is the most suitable alternative for extracting information about the anomalous Wess-Zumino term once the other parameters related to the various resonances have been measured.

The results involving the CP-odd observables have been derived under the assumptions that $f_H^I = 0$ and that its functional dependence on the kinematical variables is flat. The same assumptions have been made for the CP-even observables, but in that case, we have also assumed that $F_4 = 0$. The possibilities for testing some of these assumptions by using the observables defined in this paper have been discussed in Sec. VIII.

We have also studied the decay $\tau \to K\pi\nu_\tau$ within the context of the A2HDM and have found that the observables that we have defined may be used to test this model. In particular, we have focused on the s_2 projection of the differential width $6(-)$, comparing the range allowed by the A2HDM to that predicted by our simulation, adopting the NP parameter choice $|f_H\eta_P| = 1.79$. Using a simulation with 10^6 events, we have found that the best fit value for $f_H\eta_P^I$ obtained from the distribution is in disagreement (by more than 2σ) with the range predicted for the A2HDM. With the NP parameter choice $|f_H\eta_P| = 17.9$ and the same number of events, the disagreement between the two scenarios is much greater, and one would be able to distinguish decisively between them.

We note that a similar set of observables could be defined in order to analyze other decay modes such as $\tau^- \to \pi^-\pi^+\pi^-\nu_\tau$, $\tau^- \to K^-K^+\pi^-\nu_\tau$, and $\tau^- \to K^-K^+K^-\nu_\tau$ and their CP-conjugated decays. In fact, precise measurements of the branching ratios for these decays have already been obtained at the B-factories (see Refs. [16,18] for example).

An experimental analysis of the observables we have analyzed in this paper could be useful not only for extracting information about the resonance structure of the decay $\tau \to K\pi\nu_\tau$ but also for obtaining additional constraints on the NP pseudoscalar coupling. Moreover, with the higher luminosity expected for the upcoming super B-factories, the number of events anticipated for the decay $\tau \to K\pi\nu_\tau$ would be enough to exploit the information provided by the proposed observables.

ACKNOWLEDGMENTS

APPENDIX: STATISTICAL UNCERTAINTIES

In this appendix we summarize some results regarding statistical uncertainties associated with the distributions considered in this work.

The estimator that we have used to extract the projections onto Q^2, s_1, and s_2 of the weighted partial differential widths from the simulated events is given by

$$\frac{1}{\Gamma_{\text{tot}}} \frac{d\hat{\Gamma}_i}{dx}(x_0) = \frac{N}{N_{\text{ev}}} \frac{\bar{h}_i}{\Delta x} \mathcal{B}_{\tau \to K\pi\pi\nu_\tau}, \quad \text{(A1)}$$

where $\frac{d\hat{\Gamma}_i}{dx}(x_0)$ denotes the projection onto $x \equiv Q^2, s_1, s_2$ of the ith weighted partial width evaluated at x_0; N is the number of events within the bin $(x_0 - \Delta x/2, x_0 + \Delta x/2)$; $\bar{h}_i$ is the sample mean of the angular function $h_i(\gamma, \beta)$ (see Table I) in the bin; and N_{ev} is the total number of simulated events. We note that the presence of the branching ratio $(\mathcal{B}_{\tau \to K\pi\pi\nu_\tau})$ arises from the fact that we have normalized the observables to the total decay width (Γ_{tot}).

To estimate the statistical error associated with $d\Gamma_i/dx$, we use error propagation in Eq. (A1), taking into account the standard deviations of the number of events in a given bin, N, and of the sample mean, $\bar{h}_i$. The expression that we obtain for the jth bin is given by

$$\sigma_j = \frac{\mathcal{B}_{\tau \to K\pi\pi\nu_\tau}}{\Delta x} \frac{\sqrt{I_j}}{\sqrt{N_{\text{ev}}}} (\sigma_{h_i} + \langle h_i \rangle \sqrt{1 - I_j}), \quad \text{(A2)}$$

where $\sigma_{h_i} = \sqrt{\langle h_i^2 \rangle - \langle h_i \rangle^2}$ is the standard deviation of h_i computed for the jth bin, I_j is the probability for a given event to lie within that bin, and $\langle h_i^2 \rangle$ and $\langle h_i \rangle$ denote the mean values of h_i^2 and h_i, respectively, which are calculated, again, for the jth bin. In general, for all the observables, the dominant contribution arises from the standard deviation of the angular function, σ_{h_i}, while the second term in Eq. (A2) is negligible. The unique exception is the observable with $i = 1$, for which $\sigma_{h_1} = 0$ (due to the fact that $h_1(\alpha, \beta) = 1$—see Table I), so that the second term is the dominant one. Actually, this second term computed for the observable $d\Gamma_1/dx$ turns out to be comparable to the first contribution obtained for any of the remaining observables $(d\Gamma_i/dx, i = 2, ..., 9)$. Therefore, the statistical uncertainties σ_j are of the same order of magnitude for all of the weighted partial widths $(i = 1, ..., 9)$. Of course, the order of magnitude of the uncertainty in Eq. (A2) changes from one bin to another and from one projection to another $(x = Q^2, s_1, \text{or } s_2)$.

[1] G. Aad *et al.* (ATLAS Collaboration), Phys. Lett. B **716**, 1 (2012).

[2] S. Chatrchyan *et al.* (CMS Collaboration), Phys. Lett. B **716**, 30 (2012).

[3] J. Ellis, D. S. Hwang, K. Sakurai, and M. Takeuchi, J. High Energy Phys. 04 (2014) 004.

[4] J. Ellis and T. You, J. High Energy Phys. 06 (2013) 103.

[5] G. Aad *et al.* (ATLAS Collaboration), J. High Energy Phys. 06 (2012) 39.

[6] S. Chatrchyan *et al.* (CMS Collaboration), J. High Energy Phys. 07 (2012) 143.

[7] T. A. Aaltonen *et al.* (CDF Collaboration), Phys. Rev. D **89**, 091101 (2014).

[8] J. Beringer *et al.* (Particle Data Group), Phys. Rev. D **86**, 010001 (2012).

[9] K. Kiers, K. Little, A. Datta, D. London, M. Nagashima, and A. Szynkman, Phys. Rev. D **78**, 113008 (2008).

[10] D. M. Asner *et al.* (CLEO Collaboration), Phys. Rev. D **62**, 072006 (2000).

[11] M. Jung, A. Pich, and P. Tuzon, J. High Energy Phys. 11 (2010) 003.

[12] A. Celis, M. Jung, X.-Q. Li, and A. Pich, J. High Energy Phys. 01 (2013) 054.

[13] G. C. Branco, P. M. Ferreira, L. Lavoura, M. N. Rebelo, M. Sher, and J. P. Silva, Phys. Rep. **516**, 1 (2012).

[14] J. H. Kuhn and E. Mirkes, Z. Phys. C **56**, 661 (1992); **67**, 364(E) (1995).

[15] R. Decker, M. Finkemeier, and E. Mirkes, Phys. Rev. D **50**, 6863 (1994).

[16] I. Adachi *et al.* (Belle Collaboration), arXiv:0812.0480.

[17] R. Decker, E. Mirkes, R. Sauer, and Z. Was, Z. Phys. C **58**, 445 (1993).

[18] B. Aubert *et al.* (*BABAR* Collaboration), Phys. Rev. Lett. **100**, 011801 (2008).

[19] M. Lee *et al.* (Belle Collaboration), Phys. Rev. D **81**, 113007 (2010).

[20] H. Guler *et al.* (Belle Collaboration), Phys. Rev. D **83**, 032005 (2011).

[21] M. Finkemeier and E. Mirkes, arXiv:hep-ph/9503474.

[22] J. H. Kuhn and A. Santamaria, Z. Phys. C **48**, 445 (1990).

[23] K. Akai, Conf. Proc. **C130513**, TUYB101 (2013).